An ultrasensitive vibrating channel mass sensor based on tunnelling current detection

MAURIZIO MIGLIORE
Department of electrical engineering
EPFL - Ecole polytechnique
fédérale de Lausanne
CH-1015 Lausanne
SWITZERLAND
mauri.migliore@gmail.com

ZAKARIA MOKTADIR
School of electronics and
computer sciences
University of Southampton
SO17 1BJ, Southampton
UNITED KINGDOM
zm@ecs.soton.ac.uk

HIROSHI MIZUTA
School of electronics and
computer sciences
University of Southampton
SO17 1BJ, Southampton
UNITED KINGDOM
hm2@ecs.soton.ac.uk

Abstract: - We present a new design of a mass sensor capable of detecting mass values in the zeptogram range. The sensor comprises a resonant beam and two gate electrodes used to oscillate the beam at its resonance frequency. The detection method is based on the tunnelling current between the vibrating beam and the gate electrodes. When a small mass is added to the beam, the latter sees a shift in its resonant frequency. The added mass thus leads to a decrease in the oscillation's amplitude and hence a drop in the tunnelling current.

Key-words: - Tunneling current, NEMS, vibrating channel, mass sensor

1 Introduction

Nano-Electro-Mechanical systems (NEMS) used as sensors are gaining increasing interest thanks to their high sensitivity, small dimensions and low power consumption. In addition, these systems can be easily integrated with IC technology, for instance the CMOS process. This will allow the development of monolithic processes allowing the fabrication of ultrasensitive sensors.

Mass sensors have been the subject of intense investigation and were developed by several research groups. For instance monolithic approach to mass detection using a nano-cantilever and an integrated capacitive readout (CMOS) was demonstrated by Davis *et al* [1]. Villarroya *et al* developed a mass sensor based on an array of cantilevers fabricated on polysilicon and integrated monolithically to a CMOS circuitry [2]. Their on chip MEMS sensor allowed a mass sensitivity higher than 28 Hz/fg and a mass resolution smaller than 2 fg. A CMOS based device was also developed by Verd and co-workers, reaching a sensitivity of 0.9 ag/Hz [3]. Recent work includes the development of a bulk acoustic resonator fabricated on polysilicon, with a sensitivity of about 100 Hz/fg [4] in air.

In this paper we present a new concept which will enable ultrasensitive mass detection, exploiting the tunnelling current between a vibrating beam (the channel) and two fixed electrodes (the gate). By measuring the gate-channel tunnelling current we can theoretically reach a device responsivity to tens of zeptograms (1 zg = 10^{-21} g). This resolution is extremely high when compared to the most current mass sensors.

2 Device concept

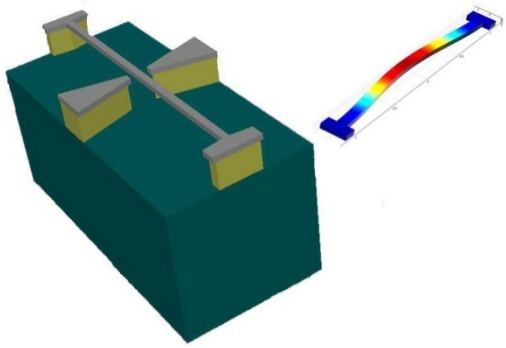

Fig.1 3D model of the device showing the two gate electrodes and the oscillating channel (the beam). The inset shows FEM modelling of the beam's in-plane oscillations.

In figure 1 we show a 3D model of a possible device structure. The inset shows FEM modelling of the beam's in-plane oscillations. This configuration can be fabricated using an SOI wafer, in which the beam and the electrodes are defined by patterning and etching of the oxide sacrificial layer. The suspended beam is then electrostatically actuated by the two electrodes at its resonance frequency.

The sensor is functionalized by coating the beam with an active material able to adsorb the compound to be detected. By applying a DC voltage to the electrodes a tunnelling current between the beam and the electrodes is created. Since this current is exponentially dependent on the distance, very small mass variations could lead to measurable changes in the tunnelling current. Any small change in the mass of the beam, due to the adsorption of the target compound would shift its resonance frequency, resulting in a decrease of

the oscillation's amplitude which in turn leads to a drop of the tunnelling current. In comparison, capacitive or optical methods would not be capable of detecting such a small change in the beam's resonant frequency.
A combination of both, the beam mechanics and a quantum mechanical description of the tunnelling current will be presented in the following sections. In the rest of the paper, we will use the geometrical parameters displayed in table 1 to derive all relevant physical quantities.

Beam length	2 μm
Beam width	75 nm
Thickness	40 nm
Electrodes width	50 nm

Table 1 Geometrical parameters used in the modelling of the device.

2 Beam mechanics

We will first determine the resonance frequency of the beam, then we will derive the beam shape under electrostatic actuation; in the last section we will discuss the response of the device to the mass variation.

2.1 Modal analysis

To obtain the resonant frequency of the oscillation we will use both an analytical model and FEM simulations. The analytical solution is obtained solving the Euler-Bernoulli beam equation, equation (1) [5], while the FEM solution is derived using COMSOL Multiphysics and CoventorWare software [6]. An undamped Euler-Bernoulli beam is described by the following equation:

$$\mathrm{E\,I}\ \frac{\partial^4}{\partial x^4}\,U(x,t) + \rho A\,\frac{\partial^2}{\partial t^2}\,U(x,t) = 0 \qquad (1)$$

Where E is the silicon's Young modulus, I is the second moment of inertia of the cross section, $U(x,t)$ is the beam deflection, ρ is the material density and A is the beam cross section area. In equation (1) we neglect the shear deformation in the principal axe of the beam. Assuming harmonic oscillations the function $U(x,t)$ can be written as: $U(x,t) = U(x)\,e^{j\omega t}$. The general solution of (1) is given by:

$$U(x) = A\cos(\beta x) + B\sin(\beta x) + Ce^{\beta x} + De^{-\beta x} \qquad (2)$$

Where A, B, C and D are constants and β is given by:

$$\beta^4 = \frac{\rho A\omega^2}{EI} \qquad (3)$$

The normal modes are determined by introducing the clamped-clamped beam boundary conditions i.e. $U(0) = 0,\ U'(0) = 0,\ U(L) = 0,\ U'(L) = 0$. This leads the following implicit equation for the normal modes:

$$\cosh(\beta L)\cos(\beta L) = 1 \qquad (4)$$

This equation is solved numerically to drive βL satisfying (4). The normal modes are then determined by plugging the values of β into equation (3). In table 2 we show the frequency of the first mode alongside the values found using commercial software.

COMSOL	143.5 MHz
CoventorWare	147.0 MHz
Math model	144.5 MHz
Average	145.0 MHz

Table 2 First in-plane oscillation eigenfrequencies derived using different methods.

As can be seen the three frequencies are very close, with a mismatch of less than 1.5 % in the worst case. In the subsequent calculations we will use the average frequency value which is 145 MHz.

2.2 Beam deflection under applied load

Under an applied load, the equation of motion of the beam is similar to equation (1) except that a source term representing the electrostatic load is introduced in the right hand side of the equation i.e. :

$$\mathrm{E\,I}\ \frac{\partial^4}{\partial x^4}\,U(x,t) + \rho A\,\frac{\partial^2}{\partial t^2}\,U(x,t) = P(x,t) \qquad (5)$$

Here $P(x,t)$ is the electrostatic force per unit length of the beam .
Assuming harmonic oscillations and a harmonic load we can write:

$$U(x,t) = U(x)\,e^{i\omega t} \qquad (6)$$

and

$$P(x,t) = P_0\,e^{i\omega t} \qquad (7)$$

With these assumptions, the general solution for the spatial component of the deflection $U(x)$ is given by:

$$U(x) = A\,\cos(\beta x) + B\,\sin(\beta x) + C\,e^{\beta x} + D\,e^{-\beta x} - \frac{P_0}{E\,I\,\beta^4} \qquad (8)$$

Where β is defined by equation (3). To obtain the coefficients A, B, C and D we will apply the boundary

conditions of zero deflection and zero slope at each beam end (clamped-clamped boundary condition) and solve the resulting linear system of equations.

2.3 Resonant frequency shift

When a small amount of mass δm is added to the beam, a shift in its resonance frequency is observed. To obtain this frequency shift we will use Rayleigh approximation i.e. the beam is treated as a harmonic oscillator with a mass m and a stiffness k. The equivalent mass and the stiffness are given by the following two relations [7]:

$$m = \int_0^L \rho A \emptyset(x)^2 dx \tag{9}$$

$$k = \int_0^L EI(\emptyset(x)'')^2 dx \tag{10}$$

where $\emptyset(x)$ is a suitable dimensionless shape function, which satisfies the same boundary condition as the general solution $U(x)$ [8]. In our calculations we neglect the electrostatic spring softening which is introduced during electrostatic actuation. We will also assume that the added mass does not change the spring constant of the beams. The approximate resonant frequency is then:

$$f_0 = \frac{\sqrt{k}}{2\pi}\frac{1}{\sqrt{m}} \propto \frac{1}{\sqrt{m}} \tag{11}$$

In this way we are able to calculate the resonance frequency shift δf for a small variation of mass δm:

$$\delta f = f_0 - f' = f_0\left(1 - \frac{1}{\sqrt{1+\frac{\delta m}{m}}}\right) \approx f_0\frac{\delta m}{2m} \quad \text{since } \delta m \ll m \tag{12}$$

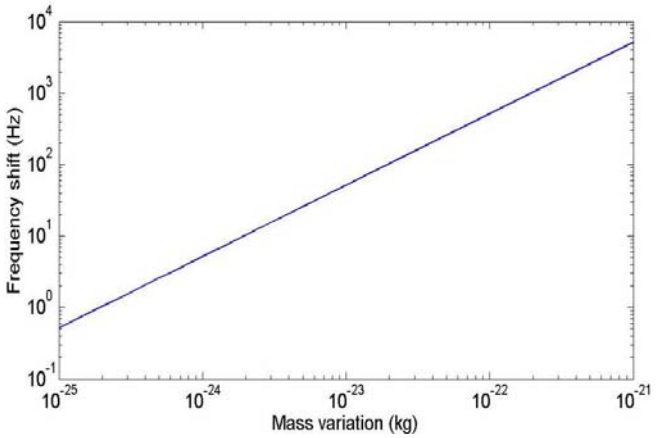

Fig.2 Frequency shift as a function of the added mass δm variation.

In figure 2 the dependence of frequency shift on δm is shown.

2.4 Near resonance beam excitation

The addition of a small mass to the beam will shift the resonance frequency from f_0 resulting in a decrease of the beam's response to the excitation. This response to a forced harmonic oscillation with a frequency ω_{ext} can be characterised by the transfer function F_T which is given by:

$$F_T = \rho\,(\omega_0^2 - \omega_{ex}^2 - i\,\omega_0\,\omega_{ex}/Q)^{-1} \tag{13}$$

here ω_0 is the beam resonance angular frequency is the excitation and Q is the quality factor. This function (normalised to its maximum value) is shown in figure 3, for Q=100.

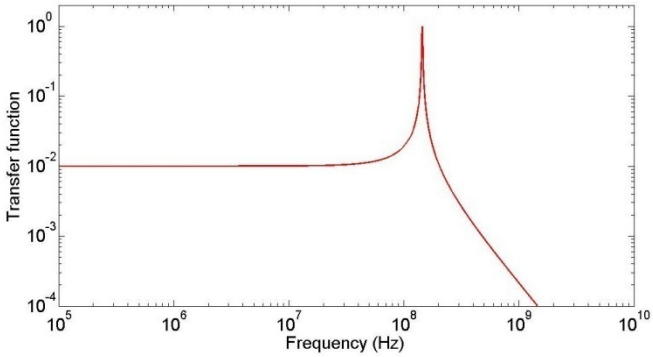

Fig.3 System transfer function for Q = 100.

Using the results above, we can estimate the value of the tunnelling current as a function of the beam deflection. It is expected that when a small entity is added to the resonant beam, a drop of the tunnelling current will be observed since the added mass drives the beam off-resonance, which results in an increase in the distance between the beam centre and the gate electrodes. These considerations will be the subject of the following sections.

3 Beam-gate tunnelling current

Here we will examine the expression of the tunnelling current between the gate electrodes and the oscillating beam. For this purpose, we will adopt the Tsu-Esaki model [9].

3.1 Transmission coefficient

When the gate electrode and the oscillating beam are few nanometres apart, tunnelling of the electrons takes place between the two media. This effect is modelled by a trapezoidal potential barrier whose height is equal to the silicon affinity χ and is tilted due to the action of the applied DC voltage across the beam and the gate electrode. Figure 4 shows a sketched energy diagram and the electronic wave function in different regions.

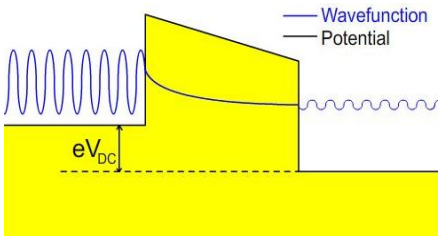

Fig.4 Sketch of the energy diagram and the tunnelling effect for the beam-electrodes system in consideration.

This phenomenon is characterised by the so called transmission coefficient, which quantifies the transmitted to incident probability flux density.
This coefficient is obtained by solving the Schrödinger equation which allows the determination of the amplitude of the transmitted wave as a function of the barrier parameters and electron energy [10]. The transmission coefficient T_c is given by the relation:

$$T_c = |D|^2 \tag{14}$$

$$D = \frac{2\, i\, q_0\, k}{\pi\, a\, \Delta}\, \eta\, e^{-ika} \tag{15}$$

Where

$$k = \sqrt{2\, m\, E/\hbar^2} \tag{16}$$

$$q_0 = (k_0\, a/\eta)^{2/3} \tag{17}$$

$$k_0 = \sqrt{2\, m\, \chi/\hbar^2} \tag{18}$$

$$\eta = 1 - \frac{\chi - V_{DC}}{\chi} \tag{19}$$

$$\Delta = G(\xi_0)F^*(\xi_a) - F(\xi_0)G^*(\xi_a) \tag{20}$$

$$\xi_0 = q_0\left(\frac{k^2}{{k_0}^2} - 1\right) \tag{21}$$

$$\xi_a = q_0\left(\frac{k^2}{{k_0}^2} + \eta - 1\right) \tag{22}$$

$$F(\xi) = i\, k\, Ai(-\xi) - \eta\frac{q_0}{a}Ai'(-\xi) \tag{23}$$

$$G(\xi) = i\, k\, Bi(-\xi) - \eta\frac{q_0}{a}Bi'(-\xi) \tag{24}$$

Here a is the width of the potential barrier, Ai, Bi Ai' and Bi' are Airy functions and their respective derivatives. The transmission coefficient T_c can then be evaluated numerically and used in the calculation of the tunnelling current.

3.2 Tunnelling current

To evaluate the tunnelling current will use the Tsu-Esaki model [9]. This model allows us to calculate the tunnelling current between two electrodes if we know the transmission coefficient of the barrier, and the material's parameters[i]. The tunnelling current density is then given by the following expression:

$$J = \frac{4\,\pi m^* kT\, e}{h^3}\int_0^\infty T_c(E)\ln\left(\frac{1 + e^{\frac{E_f - E}{kT}}}{1 + e^{\frac{E_f - E - eV_{DC}}{kT}}}\right)dE \tag{25}$$

This expression is used to evaluate the current during the beam's oscillation period.

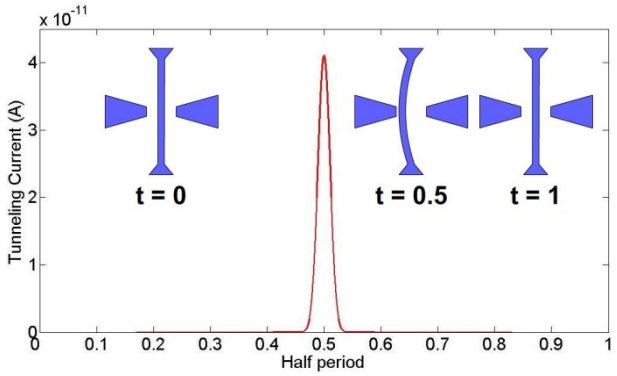

Fig.5 Tunneling current during half period of oscillation.

For our analysis we assume static tunnelling in regard to the beam's dynamics i.e. during tunnelling, electrons "see" a stationary beam.
This hypothesis is correct only if the tunnelling time is negligible with respect to the beam dynamics time scale. It is possible to calculate the expectation value of the tunnelling time for a square barrier. We will use the result from reference [11]:

$$t_{Tunn} = 2\, m\, \frac{k\,(p^2 - k^2)\, x_{max} + \frac{(p^2 + k^2)^2}{2\, k\, p}\sinh(2\, p\, x_{max})}{(p^2 + k^2)^2\cosh^2(p\, x_{max}) - (p^2 - k^2)^2} \tag{26}$$

Where $p = \sqrt{2\, m\,(\chi - E)}$ and $k = \sqrt{2\, m\, E}$; in this calculations Planck units[ii] were used. Note that this expression is derived for a square barrier and is used only to give us an order of magnitude of the tunnelling time for a tilted potential[iii]. For example, for electron energy of 0.1 eV, the tunnelling time is roughly 5.55×10^{-12} s. This value is three orders of magnitude smaller than the oscillation period (which is about 6.9×10^{-9} s in our case), for this reason we can assume the mechanical system static with respect to

[i] We considered the bottom of the conduction band as the zero energy reference and we calculated the Fermi energy for the desired doping using Fermi integrals.
[ii] In this unit system some fundamental physical constants like ħ, G and K_B are put equal to 1.
[iii] Despite the significant amount of literature published in the subject, no general consensus has yet been reached and the topic remains debatable.

the tunnelling time scale. Note also that t_{Tunn} decreases with increasing energy.
As figure 5 shows, a significant value of the tunnelling current is achieved during a small time interval i.e. when the beam is the closest to the electrode.
Having determined the expression of the tunnelling current, we will now investigate the change in its value when the mass of the beam is changed by a small amount.

4 Mass dependent current variation

Here we will investigate the relationship between the mass variation of the beam and the tunnelling current.

4.1 Excitation frequency correction

It is worth mentioning that the damping of the beam introduces a shift of the resonance frequency f_0 corresponding to the undamped beam. This shift in frequency will depend on the damping coefficient and the quality factor Q. For example using our beam data and setting Q = 100, this shift is evaluated at 3.61 kHz. The shift in resonance frequency resulting from damping is given by the following expression:

$$\delta f_{max} = f_0 \left(1 - \frac{\sqrt{4\,Q^2 - 2}}{2\,Q}\right) \qquad (27)$$

This correction is very small, but it is fundamental if we consider the frequency shift due to mass detection because it corresponds to a mass variation of about 0.7 ag which is in the range of the system responsivity.

4.2 DC polarization

We will consider the device configuration displayed in figure 6. This configuration is called the quantum shuttle [12], in which single electron behaviour and resonant tunnelling can be seen at low temperature. The aim here is to determine the tunnelling current passing through the two gaps between the beam and the two electrodes. To be able to collect a maximum current, we adopt the following set-up: the system is polarised in order to allow tunnelling only from the electrodes to the beam, and not the opposite. The current tunnelling into the beam from the two electrodes will be collected at one of the beam ends and then amplified for measurement. Figure 6 shows this concept.
With this symmetric configuration the total current per period is twice the single tunnelling current between a single gate and the beam.

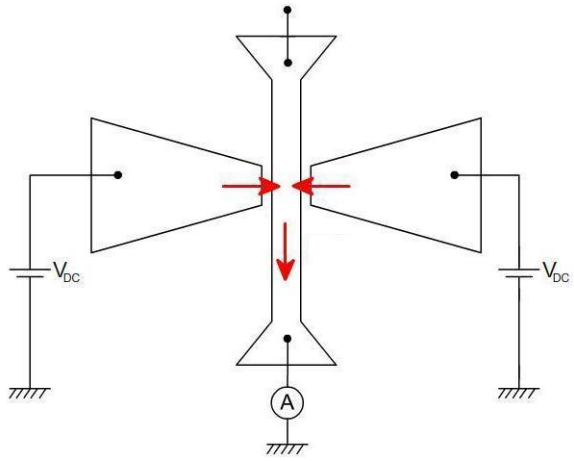

Fig.6 Quantum shuttle configuration used in this study, showing a DC polarization of the gate electrodes.

4.3 Current vs. mass relationship

We can now combine all aforementioned results to obtain the tunnelling current as a function of the sensed amount of added mass. In figure 7 we show the tunnelling current as a function of the added mass, setting Q = 100.

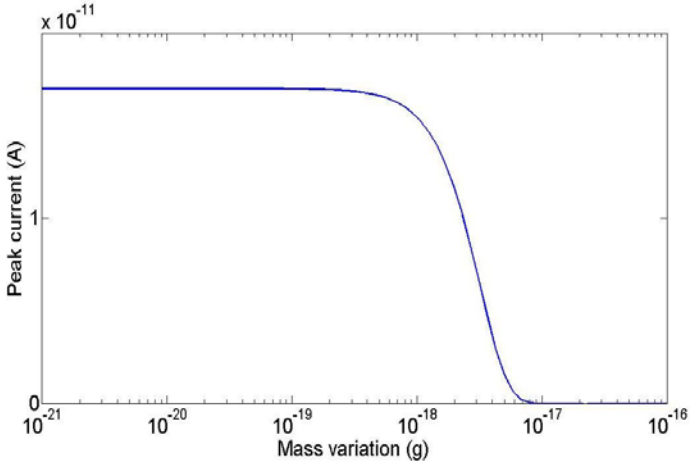

Fig.7 Added mass dependence of the tunnelling peak current.

As we can see the current has a rapid decrease from its highest value to zero within a decade of the added mass (in this example 10^{-18} – 10^{-17}). It must also be noticed that the highest responsivity is achieved within a well defined region of values of the added mass. This responsivity region can be shifted by changing the beam parameters and/or the quality factor Q. In figure 8 are reported the results for different values of the quality factor and fixed beam dimensions.

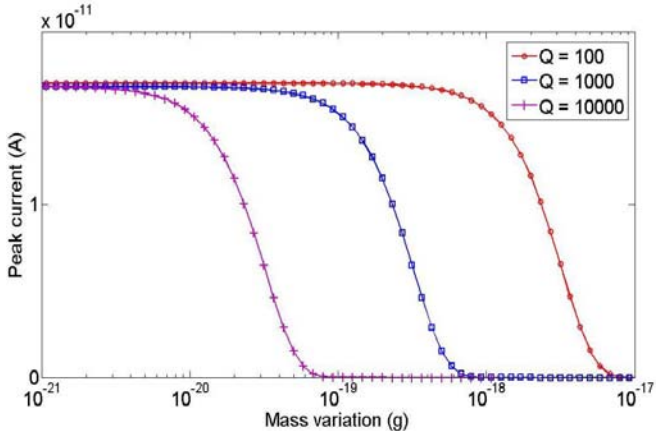

Fig 8 Mass dependence of the responsivity region as a function of the quality factor Q for fixed beam dimensions.

It is not uncommon to reach high values of the quality factors in nano-resonators. The results above show that higher values Q improve the responsivity which, in theory, can reach values up to tens of zeptograms.
Beam dimensions also affect the responsivity as well as the dynamic range. In figure 9 we show the tunnelling peak current as a function of mass variation for different beam dimensions.

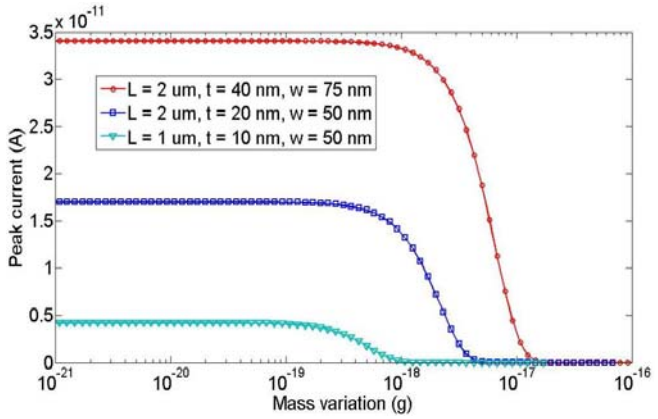

Fig.9 Tunneling peak current for different beam's dimensions

This result shows that changing the beam's dimensions leads to a shift of the dynamic range of the device. This effect can be exploited by building an array of beams, each with a different dynamic range. This will result in the increase of the responsivity to a wider range of added mass.

5 Conclusions

In conclusion, we have developed a concept of a mass sensor with responsivity in the zeptogram range. The sensing method is based on tunnelling current between a resonant channel (silicon nano-beam) and a fixed gate electrode. When a small amount of mass is attached to the beam, the latter goes off resonance, leading to a drop of the tunnelling current. Our calculations showed that the dynamic range of the sensor can be tuned by changing the beam's dimensions.
Also the responsivity of the device increases with increasing quality factor.

References:

[1] Z. J. Davis et al., *Sensors and Actuators A: Physical*, Vol. 105, No. 3, 2003, pp. 311-319
[2] M. Villarroya et al., *Sensors and Actuators A: Physical*, Vol. 132, No. 1, 2006, pp. 154-164
[3] J. Verd et al, *Appl. Phys. Lett.* , Vol. 91, 2007, pp. 013501
[4] J. H. Hales, J. Teva, A. Boisen, Z. J. Davis, *Appl. Phys. Lett.*, Vol. 95, 2009, pp. 033506.
[5] A. N. Cleland, *Foundations of Nanomechanics*, Springer Verlag, 2003.
[6] www.comsol.com, www.coventor.com
[7] C. M. Harris, A. G. Piersol Ed. *Harris's shock and vibration handbook*, 5th edition, McGraw-Hill Handbooks, 2002.
[8] R. R. Craig Jr., A. J. Kurdila, *Fundamentals of structural dynamics*, Second Edition, John Wily and Sons, 2006
[9] R. Tsu, L. Esaki, *App. Phys. Lett.*, Vol.22, 1973, pp. 562-564
[10] H. Iwamoto, V. M. Aquino, V. C. Aguilera-Navarro, *Int. J. Th. Phys.*, Vol. 42, 2003, pp. 1795-1807
[11] P. C. W. Davies, *A. J. Phys.*, Vol.73, No. 1, 2005, pp. 23-27
[12] R. H. Blick, H. Qin, H. Kim, R. Marsland, *New J. Phys.*, Vol. 9, No. 241, 2007, pp. 1-9